Nuclear Inst. and Methods in Physics Research, A 877 (2018) 293–299

Contents lists available at ScienceDirect

Nuclear Inst. and Methods in Physics Research, A

journal homepage: www.elsevier.com/locate/nima

Use of the facility EXOTIC for fusion–evaporation studies

E. Strano [a,b,*], G. Montagnoli [a,b], A.M. Stefanini [c], M. Mazzocco [a,b], G.L. Zhang [c,d], I. Zanon [a,b], G. Colucci [a,b], D. Ackermann [e], A. Boiano [h], L. Corradi [c], E. Fioretto [c], F. Galtarossa [c,f], M. La Commara [g,h], G. La Rana [g,h], C. Parascandolo [h], D. Pierroutsakou [h], F. Scarlassara [a,b], F. Soramel [a,b], D. Torresi [i]

[a] Dipartimento di Fisica e Astronomia, Università di Padova, Italy
[b] INFN, Sezione di Padova, Via Marzolo 8, I-35131 Padova, Italy
[c] INFN, Laboratori Nazionali di Legnaro, Viale dell'Università 2, I-35020 Legnaro, Italy
[d] School of Physics and Nuclear Energy Engineering, Beihang University, 100191, China
[e] GANIL, 14076 CAEN Cedex 05, France
[f] Dipartimento di Fisica e Scienze della Terra, Università di Ferrara, Ferrara, Italy
[g] Dipartimento di Scienze Fisiche, Università di Napoli, Italy
[h] INFN, Sezione di Napoli, Via Cintia, I-80126 Napoli, Italy
[i] INFN, Laboratori Nazionali del Sud, Via S. Sofia 62, I-95123 Catania, Italy

ARTICLE INFO

Keywords:
Heavy-ion sub-barrier fusion
Spectrometers and spectroscopic techniques
Particle identification
Beam optics

ABSTRACT

The EXOTIC facility was developed to produce light radioactive beams and it is installed at Laboratori Nazionali di Legnaro (LNL) of INFN. We have explored the capabilities of EXOTIC as a beam separator for studies of heavy ion fusion–evaporation reactions. For this purpose, the facility has been slightly modified to allow the detection and identification of the fusion–evaporation residues (ER). We have measured fusion reactions for the two systems $^{32}S + ^{48}Ca$ and $^{32}S + ^{64}Ni$ where the cross sections are known from previous experiments at LNL. The ion optical parameters of EXOTIC have been set to maximize the ER yield in the detector system for the various cases. A good and clean separation of the ER from beam-like particles was obtained in the experimental Energy–Time of Flight correlation plots. These encouraging results have been compared with the performance of the electrostatic deflector set-up PISOLO, routinely used at LNL for sub-barrier fusion experiments. The beam rejection factor of EXOTIC at 0°is comparable to the one of PISOLO at 2°–3°, while a gain of overall efficiency up to a factor 3 has been obtained with EXOTIC. We briefly discuss possible ways of improving these results.

1. Introduction

Near- and sub-barrier fusion of medium-mass heavy-ion systems is a subject offering ongoing interest both for experiments and for theories based on coupled-channels models [1]. Recently the hindrance phenomenon was discovered at deep sub-barrier energies [2]. Correctly describing the fusion excitation function is a complex task, because one has to properly take into account multi-phonon low-lying vibrations and transfer couplings, together with hindrance effects possibly "co-existing" in the same range of energies.

This means that fusion excitation functions should be measured for selected systems down to very small cross sections, smaller than what has been possible so far. Therefore new detector systems or new set-ups should be developed to overcome the limits of the present facilities.

The fusion excitation function of the system $^{32}S + ^{48}Ca$ was recently measured down to cross sections around $\simeq 1\mu b$ [3] by means of the set-up PISOLO, based on an electrostatic beam separator in use at the Laboratori Nazionali di Legnaro (LNL) for many years. The limitations of solid angle acceptance and beam rejection factor of PISOLO prevent investigations at even lower cross sections, but the regular behavior of the sub-barrier excitation function suggests that the hindrance effect may actually show up at lower beam energies in $^{32}S + ^{48}Ca$. This is a typical example where measuring fusion cross sections down to the 10–100 nb level would be of extreme importance, because it appears that in this system couplings to positive Q-value transfer channels determine the fusion yields at least down to the μb-level [4], that is, in the range where the hindrance phenomenon should occur.

* Corresponding author at: Dipartimento di Fisica e Astronomia, Università di Padova, Italy.
E-mail address: emanuele.strano@unipd.it (E. Strano).

https://doi.org/10.1016/j.nima.2017.10.008
Received 16 September 2017; Received in revised form 3 October 2017; Accepted 5 October 2017
Available online 13 October 2017
0168-9002/

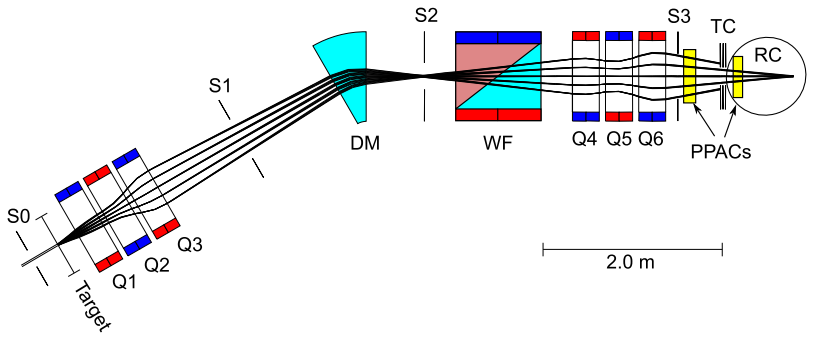

Fig. 1. Schematic view of EXOTIC consisting of a dipole bending magnet (DM), two quadrupole triplets (Q1–Q3 and Q4–Q6), a Wien filter (WF), four slit sets (S0–S3), a triple collimator (TC) a couple of parallel plate avalanche counters (PPACs) and a reaction chamber (RC).

Therefore we have considered the possibility to use the facility EXOTIC [5–9], already operating at LNL since 2004 for the production of light weakly bound Radioactive Ion Beams (RIBs), as a beam separator for detecting fusion–evaporation residues. This paper reports on the tests we have performed by measuring fusion cross sections of ^{32}S + ^{48}Ca and ^{32}S + ^{64}Ni. In the second system previous sub-barrier data were also available [10].

2. Facility description

The EXOTIC facility at the LNL, consists of a combination of eight ion-optical devices coupled with a series of slits and collimators, placed along a 8.34 m long beam line. The geometric solid angle acceptance of the facility is $\Delta\Omega = 10$ msr. A schematic representation of EXOTIC is shown in Fig. 1.

2.1. Ion optics

Optical elements.

A first quadrupole triplet (Q1–Q3), whose purpose is the enhancement of the collection acceptance for the reaction products, is located 248 mm downstream the production target. The maximum applicable magnetic field at the pole tips of the Q1–Q3 triplet is 660 mT, allowing a maximum achievable transmission for reaction products with magnetic rigidities up to $B\rho \simeq 0.635$ Tm. Unwanted nuclear species (i.e. scattered primary beam and the products of other direct reactions) are filtered by means of a 30°-bending dipole magnet (DM), which allows magnetic fields up to $B^{max}_{DM} = 1.4$ T and is placed at about 2.29 m downstream Q1 – Q3 triplet. A second quadrupole triplet (Q4–Q6), with the same characteristics as the Q1 – Q3 triplet, located 394 mm upstream from the reaction chamber (RC), is employed to focus the reaction products on the final focal plane. A velocity selection of the reaction products is performed by means of a 1 m long Wien Filter (WF), located between DM and the Q4–Q6 quadrupole triplet. The maximum voltage applied to the WF electrodes, separated by a 0.05 m gap, is $V^{max}_{WF} = \pm 50$ kV, whereas the maximum magnetic field between the two poles, separated by a 0.2 m gap, is $B^{max}_{WF} = 0.08$ T.

Slits.

Four slit sets are located along the EXOTIC facility and are mounted on movable arms, allowing the fine adjustment of their apertures, a. A four-sector slit S0 (typically $a_{0,x} = \pm 2$ mm, $a_{0,y} = \pm 2$ mm) is placed ~200 mm upstream the target to define the primary beam spot size and to simplify the centering and focusing procedures of the incident beam. The four-jaw S1 slit (usually $a_{1,x} = \pm 50.0$ mm, $a_{1,y} = \pm 20.0$ mm) is installed ~1 m upstream the DM and prevents the particles produced with marginal trajectories from hitting the inner walls of the dipole magnet chamber. Right after the DM, a two-sector slit S2 (with a standard aperture of $a_{2,x} = \pm 2.5$ mm, $a_{2,y} = \pm 10.0$ mm) is employed to select the proper $B\rho$ window of the reaction products. A fourth slit set S3 (with an usual aperture of $a_{3,x} = \pm 30.0$ mm $a_{3,y} = \pm 30.0$ mm) is placed 136 mm downstream the exit of quadrupole Q6. A triple collimator (TC), consisting of three $\phi = 20$ mm diaphragms, is placed at the entrance of the reaction chamber (RC). Finally, two position-sensitive, high-transparency Parallel Plate Avalanche Counters [11] (PPACs), placed 909 mm (PPACA) and 365 mm (PPACB) upstream the reaction target, are devoted to the tracking of the produced RIBs and to give the reference time for Time-of-Flight measurements.

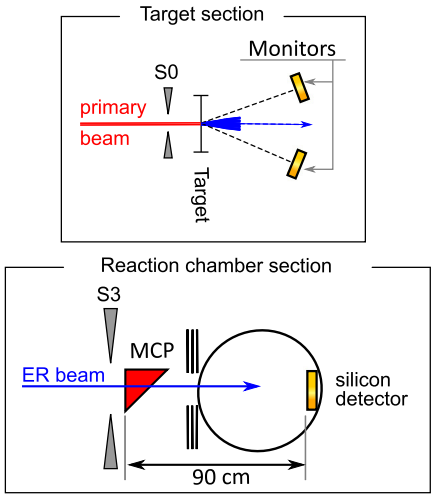

Fig. 2. Schematic view of the experimental setup employed for the fusion–evaporation studies with the EXOTIC facility. In the upper panel, the EXOTIC gas target was replaced by solid targets and two monitor detectors were installed. In the EXOTIC reaction chamber section (lower panel) an Energy/Time-of-flight telescope was used, consisting of an MCP and a Silicon detector.

2.2. Experimental setup

Few changes were made to the ordinary setup in order to test the capabilities of the EXOTIC facility as a separator for fusion–evaporation products. The target section was modified as shown in the upper panel of Fig. 2. The cryogenic gas target, described in [7], was replaced by a target holder containing a 50 μg/cm^2 thick $^{48}CaF_2$ (96.56% enriched) target and a ^{64}Ni (96.57% enriched) target, both evaporated on a 15 μg/cm^2 carbon backing. Two Silicon Surface Barrier Detectors (SSBD) were placed at θ_{lab} ~22° and at a distance of 90.2 mm from the target position to monitor the beam conditions and to normalize the ER events to the Rutherford cross section.

The detector set-up was modified as shown in the lower panel of Fig. 2. The two PPACs of the EXOTIC facility were removed whereas an Energy/Time-of-Flight telescope, consisting of a 50 mm(x) × 30 mm(y) Micro Channel Plate (MCP) detector [12] and a large area (~600 mm^2)

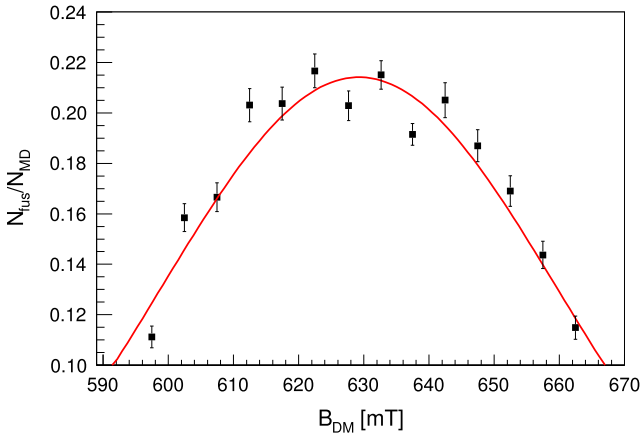

Fig. 3. Optimization of the dipole magnet by measuring the N_{fus}/N_{MD} ratio as a function of the magnetic field. A Gaussian best-fit of the N_{fus}/N_{MD} ratio is indicated by the solid line.

Table 1
Calculated and experimental values of the magnetic field for the six quadrupole lenses of the EXOTIC facility. The first column reports the calculation performed under the condition Q1=Q3 and Q4=Q6, the second column reports the calculation made imposing the condition Q1=Q3 and Q4=$Q4_{Exp}$. In the third column are listed the experimental values which maximized the transmission. Positive and negative magnetic fields indicate a *x*-focusing and a *y*-focusing quadrupole respectively.

E_{lab} 84 MeV	B_{GICOSY} [mT]	B_{GICOSY} [mT] (Q4 fixed)	B_{Exp} [mT]
Q1	278.3	278.3	264.8
Q2	−476.0	−476.0	−478.2
Q3	278.3	278.3	271.1
Q4	233.7	183.1	183.1
Q5	−393.9	−384.5	−409.8
Q6	233.7	269.3	293.9

SSBD, was installed. The MCP was located ~100 mm downstream the S3 slit set, whereas the silicon detector was placed at the far end of the reaction chamber, defining a ~900 mm long flight path.

The XTU Tandem accelerator provided a ^{32}S beam with energies in the 77–84 MeV range and intensities between 4 and 20 pnA. The investigated energy range was selected in order to match the existing data sets for the $^{32}S + {}^{48}Ca, {}^{64}Ni$ systems [3,10].

3. Experimental results

3.1. Evaporation residues selection

As a first step, the ion-optical magnetic elements of the EXOTIC facility were optimized for the $^{32}S + {}^{48}Ca$ reaction at the highest energy (84 MeV). Initial values for the magnetic fields of the quadrupole triplets and the dipole magnet were computed using the GICOSY code [13,14]. In order to match the number of free variables to the number of equations, the conditions Q1=Q3 and Q4=Q6 were imposed in the calculations. The optimization of each ion-optical element was individually performed by scanning the magnetic field around the calculated value. The ratio N_{fus}/N_{MD} between the fusion–evaporation residues (N_{fus}) and the elastic scattering events counted by the monitor detectors (N_{MD}), was hence determined for each magnetic field in the scanned range.

DM optimization. The dipole magnet was optimized setting the magnetic fields at the pole tips of the quadrupole lenses at the calculated values reported in the first column of Table 1 (B_{GICOSY}). Fig. 3 shows the ratio N_{fus}/N_{MD} as a function of the magnetic field on the Magnetic Dipole. In the scanned range, a Gaussian best-fit was performed in order to define the central value B_{DM} = 629.3 mT.

Q1–Q3 optimization. The optimization of the magnetic fields for the first quadrupole triplet was performed in a range of about 50–80 mT around the value calculated by GICOSY (first column of Table 1). Deviations up to a maximum of about 5% with respect to the experimental values (third column of Table 1) were observed, highlighting the accuracy of the ion optical calculation and the remarkable alignment of the magnets along the beam line. The first three plots of Fig. 4 show the result of the scanning on the Q1–Q3 quadrupole triplet.

Q4–Q6 optimization. Larger magnetic field ranges were scanned for the Q4–Q6 quadrupole triplet. The difference between the experimental magnetic field intensity of the Q5 triplet and the calculated value resulted to be about 2.5%. In the optimization procedure for the Q4 quadrupole a discrepancy of about 25% was noticed between the calculated and the experimental value which guaranteed the maximum transmission. A similar difference, but in the opposite direction, was observed for the Q6 quadrupole and might be related to a possible residual misalignment of the quadrupole triplet axis with respect to the evaporation residue trajectory. In order to compensate this effect and guarantee a higher transmission, the magnetic field at the pole tips of Q4 quadrupole was therefore decreased approximately by 60 mT, whereas the magnetic field at the pole tips of Q6 quadrupole was increased by the same amount. Since the ion-optical alignment was checked employing a laser-assisted tracking system, this issue needs further investigations in new tests for the same reaction and also for a different primary beam. Additional ion-optics calculations were performed letting free Q5 and Q6 but imposing the experimental value of Q4 (and preserving the condition Q1=Q3 in the first quadrupole triplet) in the GICOSY input. The second column of Table 1 reports the calculation results which, in the case of the Q6 quadrupole, exhibit a discrepancy that is reduced by a factor of 2 with respect to the initial calculation. Fig. 4 shows the ratio N_{fus}/N_{MD} for the six quadrupole magnets as a function of the magnetic field.

The magnetic fields for the bending dipole and quadrupole triplets, after being tuned for the $^{32}S + {}^{48}Ca$ collisions at 84 MeV, were scaled for the other energies and the $^{32}S + {}^{64}Ni$ reaction according to the selected magnetic rigidity of the evaporation residues, calculated using the code PACE4 [15].

3.2. Wien filter optimization

The Wien Filter optimization was performed setting the electrodes voltage to ±8 kV and scanning the magnetic field in the 34–41 mT range. The procedure was repeated for three different magnetic fields of the DM: 628.2 mT (close to the central value in Fig. 3), 623.0 mT and 633.2 mT. Fig. 5 shows the N_{fus}/N_{MD} ratio as a function of the magnetic field in the Wien Filter.

The lines in Fig. 5 correspond to the best fits of the collected data and, as it can be clearly seen, the three centroids are nicely consistent with each other. The mean value of the three data sets (37.64 mT) was later properly scaled for the other energies and the $^{32}S + {}^{64}Ni$ reaction according to the selected velocity of the evaporation residues as tabulated in Table 2.

3.3. Wien filter transmission

A further test was performed in order to investigate the effects of the electric field across the Wien filter electrodes on the transmission. Fig. 6 shows the N_{fus}/N_{MD} ratio for three different voltages applied to the WF electrodes (V_{WF} = ±8 kV, ±12 kV, ±16 kV) as a function of the B_{WF}/V_{WF} ratio between the magnetic field (B_{WF}) and the voltage (V_{WF}) applied to each electrode. The B_{WF}/V_{WF} ratio is essentially proportional to the velocity of filtered reaction products. Fig. 6 indicates that the voltage V_{WF} = ±8 kV ensures the highest transmission value through the apparatus.

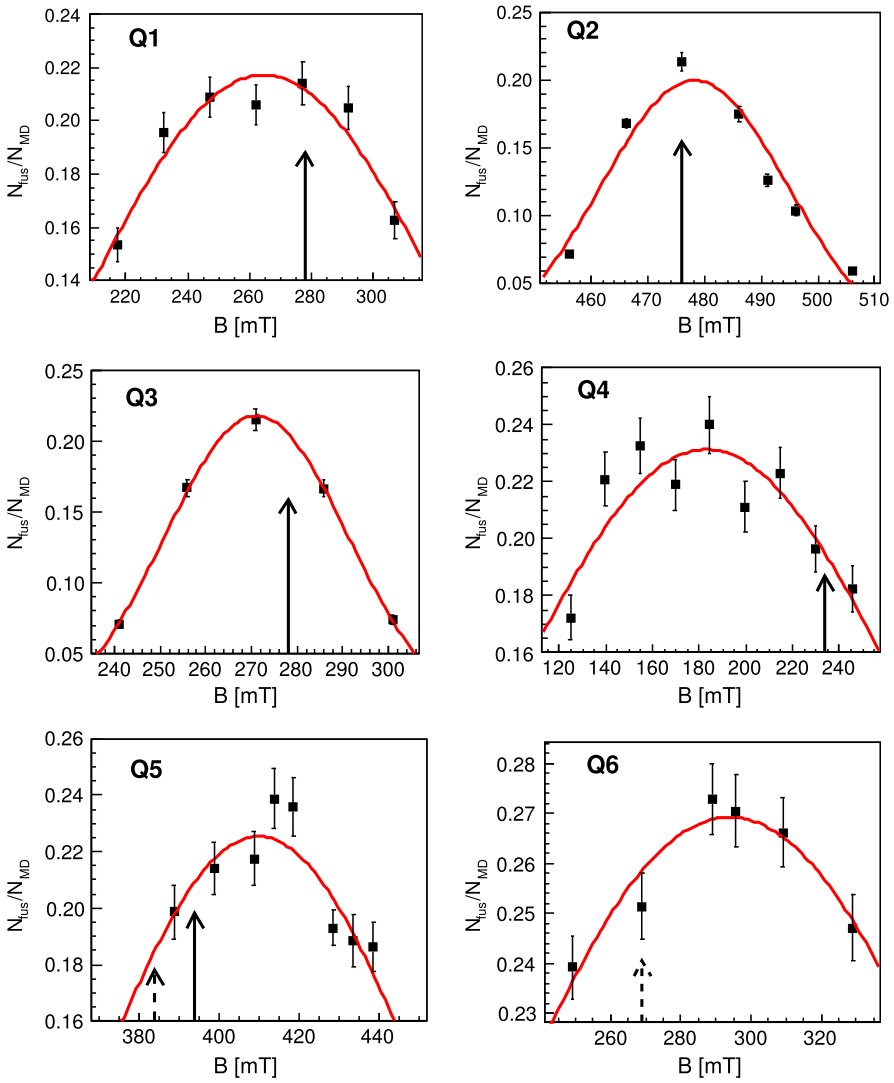

Fig. 4. Optimization of the quadrupole lenses by measuring the N_{fus}/N_{MD} ratio as a function of the magnetic field in the scanned range. The solid lines correspond to Gaussian best-fits. The dashed arrows are the calculated values with the conditions Q1=Q3 and Q4=Q6. The solid arrows indicate the values calculated with the conditions Q1 = Q3 and Q4=$Q4_{Exp}$ (see the text for additional details).

3.4. Slit optimization

The left panel of Fig. 7 displays the N_{fus}/N_{MD} ratio as a function of the S2 slit aperture. As it can be observed, the ratio increases linearly up to an opening of ±5 mm. As the slit is further opened, the ratio still get larger but with a less steep trend and then it seems to saturate at a S2 slit aperture of about ±8–10 mm.

The right panel of Fig. 7 shows the optimization procedure of the S3 slit for two S2 apertures (±5 mm and ±10 mm). In this case, the N_{fus}/N_{MD} ratio increases almost linearly for both the S2 apertures up to ±15 mm, then the increase is much weaker, indicating that the evaporation residue with marginal trajectories at S3 have a rather low probability to pass through the triple collimator (ϕ = 20 mm) at the entrance of the reaction chamber and to reach the focal plane detector.

4. Excitation functions of $^{32}S+^{48}Ca,^{64}Ni$

Some examples of the results obtained in the runs are reported in Figs. 8 and 9. The spectra are clean and the ER are clearly separated from the residual beam-like particles. Both in the ER groups and in the long lines where the residual beam events show up, we can notice two-three main structures corresponding to different ion charge states. The measurement at 78 MeV for $^{32}S+^{64}Ni$ corresponds to a cross section of ≃13 μb and the few ER events shown in the upper panel of Fig. 9 have been collected in a 8 h run with a beam intensity of 9 pnA.

Table 2
Wien filter magnetic fields for the $^{32}S+^{48}Ca,^{64}Ni$ collisions at four energies in the laboratory reference frame as a function of the velocity of the selected evaporation residues. The voltage across the Wien filter was fixed at ±8 kV.

V_{WF} = ±8 kV	$^{32}S+^{48}Ca$		$^{32}S+^{64}Ni$	
Elab [MeV]	v [cm/ns]	B_{WF} [mT]	v [cm/ns]	B_{WF} [mT]
77	0.84	39.36	0.70	47.17
78	0.85	39.20	0.71	46.87
81	0.86	38.44	0.72	45.96
84	0.88	37.64	0.74	45.11

A qualitative comparison has been carried out with the performance of the electrostatic deflector set-up PISOLO [12] usually employed for sub-barrier fusion measurements at LNL. First we have considered the primary beam rejection factor defined as the ratio between the number of beam particles impinging on the target, and the number of detected beam and beam-like ions in the same time period.

The rejection factors measured with EXOTIC in the present tests are 2–6×10^8 and 2–6×10^9 for $^{32}S+^{48}Ca$ and $^{32}S+^{64}Ni$, respectively, depending on the beam energy. These values are comparable with those

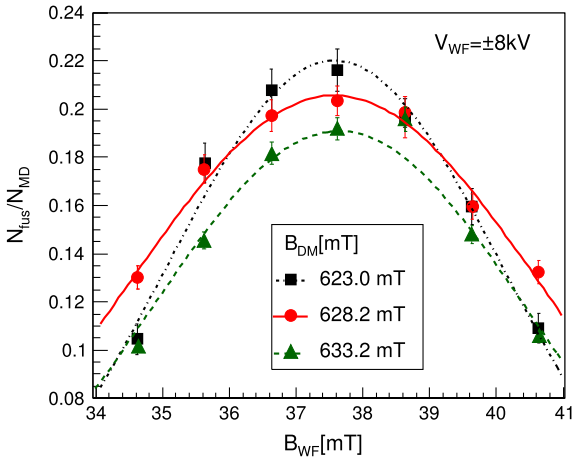

Fig. 5. (Color version online) optimization of the magnetic field of the Wien filter by measuring the N_{fus}/N_{MD} ratio as a function of the magnetic field in the scanned range. The scanning procedure was repeated for three different values of the dipole Magnet field: 623.0 mT (black squares), 628.2 mT (red circles), 633.2 mT (green triangles). The lines represent the Gaussian best-fits for the three data sets.

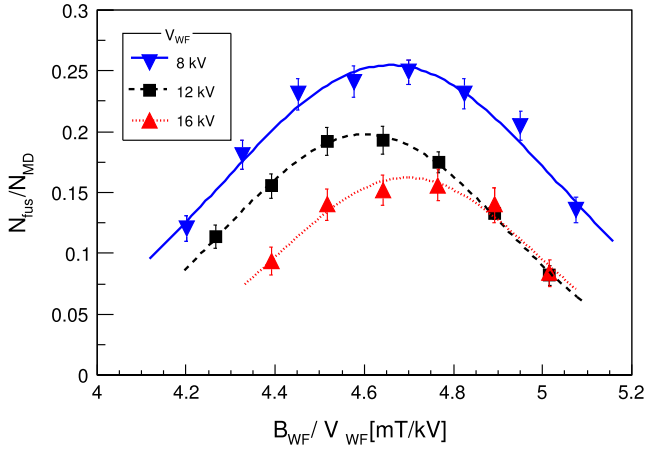

Fig. 6. (Color version online) optimization of the electric and magnetic field of the Wien filter by measuring the N_{fus}/N_{MD} ratio as a function of the ratio between the magnetic field B_{WF} and the potential applied to the WF poles V_{WF}. The procedure was repeated for three different V_{WF} values: ±8 kV (blue downside triangle), ±12 kV (black squares), ±16 kV (red upside triangles). Lines correspond to the Gaussian best-fits of the three data sets.

obtained routinely with PISOLO. However, one has to take into account that the electrostatic deflector is normally operated at 2°–3° to obtain matrices of quality and cleanliness analogous to those shown in Figs. 8 and 9. In the present tests EXOTIC was operating at 0° where the background conditions are obviously much worse.

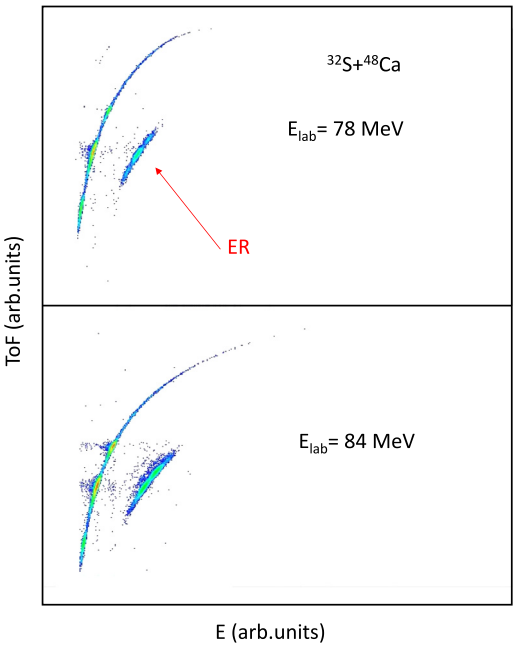

Fig. 8. (Color version online) energy–time of flight matrices measured during the test with $^{32}S + ^{48}Ca$ reaction. The red arrow indicates the group of fusion–evaporation residues events. The voltage of the Wien filter was ± 8 kV.

We have also tested the absolute detection efficiencies of the two set-ups (EXOTIC and PISOLO). The absolute efficiency is defined as the ratio of the number of detected ER events with respect to the number of ER produced in the target (during a given time). This second number was evaluated on the basis of the beam current, the target thickness and the known fusion cross section. The efficiency of EXOTIC has been deduced to be around $1–2\times10^{-3}$ (depending on the beam energy and on the system) in the present test runs. This is higher by a factor up to ≃3 with respect to PISOLO, and it could be further increased by using a lower voltage in the Wien filter as far as the rejection factor remains good enough to unambiguously select the ER events. Alternatively one could install a larger solid angle detector telescope, exploiting the very large geometrical solid angle of the EXOTIC set-up (≃10 msr).

The ER yields (related to the monitors counts) have been compared to the fusion cross sections obtained in the previous experiments by normalizing the results at the highest energy, for each system. Fig. 10 shows the excitation functions obtained in this way, and a good agreement is observable for both systems at all lower energies. This indicates that the transmission of EXOTIC is essentially independent of the beam energy for both systems, thus allowing, identification of fusion events at the lowest part of the excitation function with EXOTIC

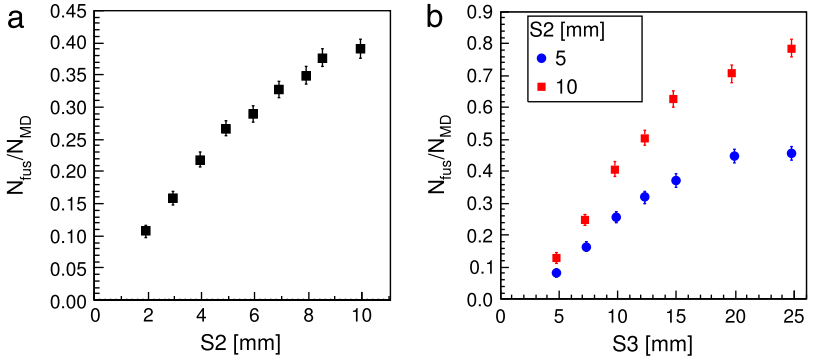

Fig. 7. (Color version online) optimization of the S2 (left panel) and S3 (right panel) slits by measuring the N_{fus}/N_{MD} ratio as a function of slit aperture.

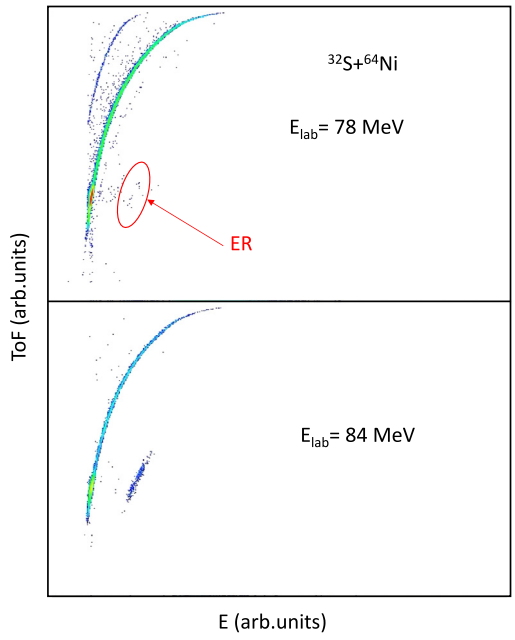

Fig. 9. (Color version online) same as Fig. 8 but for the ^{32}S + ^{64}Ni reaction.

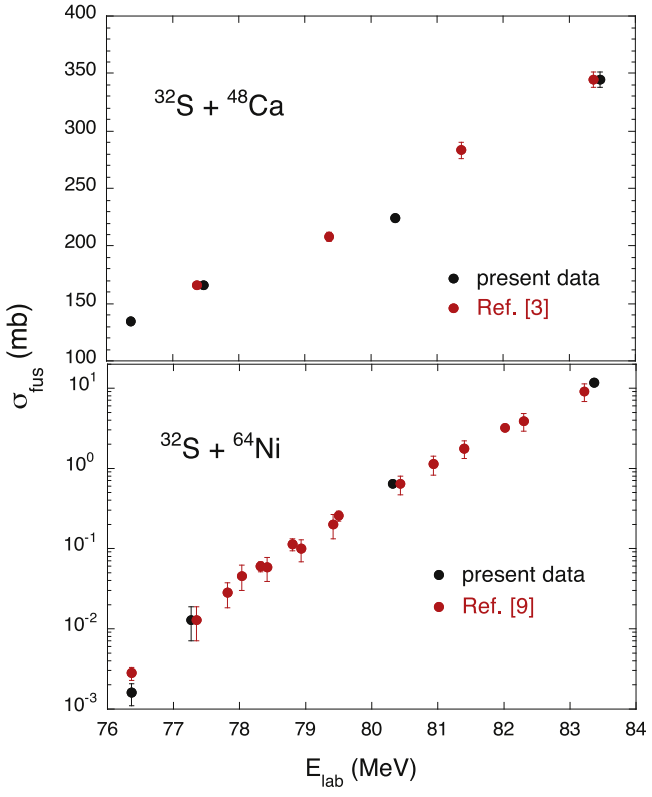

Fig. 10. (Color version online) fusion cross sections obtained in the present test compared to the already existing values for the two reactions [3,10]. The plotted laboratory energies are corrected for the energy loss in the two targets.

while normalizing the results at some higher energies with absolute cross sections obtained with PISOLO.

5. Summary

EXOTIC is a facility operating at LNL for the production of light weakly bound radioactive beams. We have demonstrated the feasibility of fusion–evaporation studies with this set-up by using it as a beam separator and ER selector. To this end, a few minor modifications were made in the detector set-up of EXOTIC. We have measured fusion cross sections for the two systems ^{32}S + ^{48}Ca and ^{32}S + ^{64}Ni, where previous data were obtained using the electrostatic deflector of LNL. The ^{32}S beam was delivered by the XTU tandem accelerator at a few energies in the range 77–84 MeV.

The ion-optical magnetic elements of the EXOTIC facility have been optimized for the ^{32}S + ^{48}Ca reaction at the highest measured energy (84 MeV). Initial values for the magnetic fields of the quadrupole triplets and the dipole magnet were computed using the GICOSY code [13,14]. The optimization of each ion-optical element was individually performed by scanning the magnetic field around the calculated value. The electrodes voltage of the Wien filter was optimized as a function of the dipole magnet field, to obtain the highest transmission through the device.

Clean E-ToF spectra were measured where the ER events were clearly identified at all energies. Beam rejection factors larger than 10^8 and 10^9 have been obtained for ^{32}S + ^{48}Ca and ^{32}S + ^{64}Ni, respectively. These values measured at 0° are comparable with those routinely achieved with PISOLO that, however, is operated at 2°–3° where the background conditions are “a priori” much more favorable. On the other hand the ER detection efficiency for EXOTIC is a factor up to 3 better than for PISOLO.

As a conclusion of this work, we point out that optimizing the fields inside the Wien filter is very important since a higher field results in a higher rejection factor, but it also decreases the transmission of the device. The loss of efficiency may be compensated by using bigger detectors, by exploiting the very large geometric solid angle of the EXOTIC set-up. This would possibly allow experiments on fusion cross sections down to the sub-μb range, where the interesting phenomenon of fusion hindrance usually shows up most clearly. Measuring absolute fusion cross sections will certainly require performing reliable simulations of the transmission of the whole set up in the various cases of interest, for a range of energy and for the several evaporation channels although this has not yet been demonstrated.

As an alternative, we can consider to carry out combined experiments using PISOLO near the barrier for absolute cross section normalization and EXOTIC at the lower energies where the better performance of this set-up would be very useful.

Acknowledgments

We acknowledge the professional work of the XTU Tandem staff, and of M. Loriggiola for preparing targets of excellent quality. This work has been partially supported by the University of Padua under the “Progetto di Ricerca di Ateneo” CPDA145301.

References

[1] B.B. Back, H. Esbensen, C.L. Jiang, K.E. Rehm, Recent development in heavy-ion fusion reactions, Rev. Mod. Phys. 86 (2014) 317.
[2] C.L. Jiang, et al., Unexpected behaviour of heavy-ion fusion cross sections at extreme sub-barrier energies, Phys. Rev. Lett. 89 (2002) 052701.
[3] G. Montagnoli, et al., Effects of transfer channels on near- and sub-barrier fusion of ^{32}S + ^{48}Ca, Phys. Rev. C 87 (2013) 014611.
[4] H. Esbensen, G. Montagnoli, A.M. Stefanini, Revised analysis of ^{40}Ca + ^{96}Zr fusion reactions, Phys. Rev. C 93 (2016) 034609.
[5] V.Z. Maidikov, et al., The optics of the exotic beam line at LNL, Nucl. Phys. A 746 (2004) 389–392.
[6] D. Pierroutsakou, et al., Light radioactive nuclear beams at LNL, Europ. Phys. Jour. Spec. Topics 150 (1) (2007) 47–50.
[7] M. Mazzocco, et al., Upgrade of the facility {EXOTIC} for the in-flight production of light radioactive ion beams, Nucl. Inst. Meth. B 317 (2013) 223–226.
[8] F. Farinon, et al., Commissioning of the {EXOTIC} beam line, Nucl. Inst. Meth. B 266 (19–20) (2008) 4097–4102.
[9] M. Mazzocco, et al., Production and separation of light low-energy radioactive ion beams with the {EXOTIC} beam-line at {LNL}, Nucl. Inst. Meth. B 266 (19–20) (2008) 4665–4669.

[10] A.M. Stefanini, et al., Heavy-Ion fusion below the Coulomb barrier, Nucl. Phys. A 456 (1986) 509.
[11] D. Pierroutsakou, et al., The experimental set-up of the RIB in-flight facility EXOTIC, Nucl. Instr. Meth. Phys. Res. A 834 (2016) 46–70.
[12] A.M. Stefanini, et al., Fusion hindrance for ^{58}Ni + ^{54}Fe, Phys. Rev. C 82 (2010) 014614.
[13] M. Mazzocco, et al., MOCADI.FUSION: Extension of the Monte–Carlo code {MOCADI} to heavy-ion fusion– evaporation reactions, Nucl. Inst. Meth. B 266 (15) (2008) 3467–3480.
[14] M. Berz, et al., {COSY} 5.0 — The fifth order code for corpuscular optical systems, Nucl. Inst. Meth. A 258 (3) (1987) 402–406.
[15] A. Gavron, Statistical model calculations in heavy ion reactions, Phys. Rev. C 21 (1980) 230–236.